

Field excitation in fuzzy dark matter near a strong gravitational wave source

Shreyansh S. Dave*¹ and Sanatan Digal†^{1,2}

¹*The Institute of Mathematical Sciences, Chennai 600113, India*

²*Homi Bhabha National Institute, Training School Complex, Anushakti Nagar, Mumbai 400085, India*

The axion-like particles with ultralight mass ($\sim 10^{-22}$ eV) can be a possible candidate of dark matter, known as the fuzzy dark matter (FDM). These particles form Bose-Einstein condensate in the early Universe which can explain the dark matter density distribution in galaxies at the present time. We study the time evolution of ultralight axion-like field in the near region of a strong gravitational wave (GW) source, such as binary black hole merger. We show that GWs can lead to the generation of field excitations in a *spherical shell* about the source that eventually propagate out of the shell to minimize the energy density of the field configuration. These excitations are generated toward the end of the merger and in some cases even in the ringdown phase of the merger, therefore it can provide a qualitatively distinct prediction for changes in the GW waveform due to the presence of FDM. This would be helpful in investigating the existence of FDM in galaxies.

PACS numbers:

I. INTRODUCTION

The fuzzy dark matter (FDM) is considered to be one of the most promising candidates of dark matter. In this model, the field is considered to be ultralight scalar field with mass $m \sim 10^{-22}$ eV which forms Bose-Einstein condensate (BEC) at the early stage of the Universe [1–3]. Due to a very high occupation number in galactic halos, this field behaves like a classical field [1]. It has been shown that the axion-like field (pseudo-goldstone boson) with ultralight mass can be a good possible field description for such ultralight particles [4]. Since the mass of the particles in this model is very small, the corresponding de Broglie wavelength is of the astrophysical scales. Below this scale, the *uncertainty principle* leads to the stability of density perturbations in FDM against the gravitational collapse [1]. In this way, this model of dark matter resolves the overprediction in the number of substructures in dark matter halos and *cuspy core problem* that arise with the WIMPs model (weakly interacting massive particles model) of dark matter [1, 2].

As the FDM is expected to be present in the form of granular structure (of length scale ~ 1 kpc) inside the galactic halos [5], where in the background of this medium other astrophysical events, e.g., binary black hole (BBH) mergers, binary neutron star (BNS) mergers, and supernova (SN) explosions, could be occurring, and generating a strong gravitational waves (GWs). Therefore, a natural question arises that whether such a GW source has any effect on FDM, or whether FDM can affect the source so that the produced GWs get modified with observable changes in the waveform. In this regard, the following are the phenomena that have been

discussed in the literature. The exponential growth of occupation number of ultralight scalar bosons near a rotating BH or NS has been extensively studied under the phenomenon of superradiance instabilities [6–12]. This creates a bosonic cloud around such objects, which causes their spin-down [6]. In addition, it has been argued that the level transitions between quantum states of such bosonic cloud, axions (that constitute the bosonic cloud) annihilation to gravitons, and bosonova collapse of the cloud can produce observable GW signals [13, 14]. The first two processes produce long-lasting monochromatic GW signals, while the last process produces the signal which is expected to be in the distinct pattern of spikes separated by periods of time [14]. Further, under these phenomena, various prospects of probing and constraining the ultralight bosons with GWs detection at LIGO and LISA have been proposed [15–23].

When such a rotating BH or NS is part of a binary, the presence of bosonic clouds affects the inspiral motion of the binary leading to an observable signal in the GW waveform on Earth [24, 25]. In addition, the possibility of resonance transitions between the growing and decaying modes of the cloud make the cloud+binary system much more interesting [26–28]. These resonances occur when the orbital frequency of binary matches the energy difference between growing and decaying modes of the cloud. This depletes the cloud by an amount that depends on the parameters of cloud+binary system, causing the generation of a greatly enhanced and short-lived monochromatic GWs [26–29], which terminate much before the binary merger [26] (the time duration of resonance transition is set by $\Delta\Omega/\gamma$, where $\Delta\Omega$ is the resonance bandwidth for transition, and γ is the rate of change of orbital frequency of binary [28]). This phenomenon can be used to set some observational constraints on the ultralight axion-like particles [29], e.g., the observations of decay in orbital period of binary can set a bound on the decay constant of ultralight axion-like particles [30], and

*shreyanshsd@imsc.res.in

†digal@imsc.res.in

on parameters of axions in general [31]. In presence of a dark matter medium, the dephasing in GW waveform has also been studied [32]. The various prospects for axion searches with Advanced LIGO through binary mergers are discussed in detail in [33]; see refs.[34, 35] for review.

In addition to the above effects of binary merger and FDM on each other, our work in ref.[36] suggests an interesting possibility of generation of field excitations in FDM near a strong GW source, which can affect the GW waveform toward the end of the merger and in some cases even in the ringdown phase of the merger. This does not require superradiance instabilities induced by rotating BH or NS (though, the presence of bosonic clouds generated due to superradiance instabilities may have additional effects on it). Rather, the generation of field excitations due to the phenomenon discussed in ref.[36] is quite general which only requires a strong GW source that produces GWs of significantly large frequency, strain amplitude, and duration.

In ref.[36], it has been shown that a sustained spacetime oscillations can excite a complex scalar field in symmetry broken phase through *parametric resonance*. The spacetime oscillations directly couple to the momentum of field-modes, which leads to the generation of field excitation even at frequencies much smaller than the mass of longitudinal-modes of the field. In the low frequency regime, mainly transverse excitations are generated as the modes corresponding to these excitations have zero mass. The field undergoes parametric resonance if appropriate momentum-modes of the field corresponding to the frequency of spacetime oscillations are present initially. It also has been shown that the finite size effects of system set a lowest frequency cut-off to induce this phenomenon: only those spacetime oscillations are able to excite the field whose angular frequency is $\omega \gtrsim 4\pi/L$, where L is the system size [36]. This arises due to the fact that the momentum-modes having wavelength larger than the upper cut-off $\lambda_L = L$ cannot grow under the resonance process.

However, in the case of explicit symmetry breaking, in addition to finite size effects, the lowest frequency cut-off to excite the field under spacetime oscillations is also set by the mass of pseudo-goldstone boson [36]. In the case of ultralight axion-like field, the mass of pseudo-goldstone boson is $m \sim 10^{-22} \text{eV}$. Therefore to excite the most dominant resonance modes of this field, the frequency of spacetime oscillations must be $\omega \gtrsim 0.1 \text{ }\mu\text{Hz}$ or equivalently $f_{\text{GW}} \gtrsim 10 \text{ nHz}$, where $f_{\text{GW}} = \omega/2\pi$ is the frequency of GWs. This required frequency is easily achieved by various GW sources, such as BBH mergers, which can produce GWs with a maximum frequency of up to $\sim 1 \text{ kHz}$ with significantly large strain amplitude. Further, the ultralight bosons can have a wide range of possible masses between 10^{-33}eV to 10^{-10}eV [37, 38]. Therefore for the above maximum frequency produced by the binary merger systems, the upper mass cut-off of the field that can be ex-

cited by the passing of GWs will be $m \sim 10^{-11} \text{eV}$. Thus, GWs produced by binary mergers can excite ultralight axion-like field having almost all possible mass range, except for the field that has a much larger mass. Therefore, this phenomenon is certainly not possible for higher mass QCD axions as in such case the required GW frequency would be way beyond the reach of any known GW source with significantly large strain amplitude (for a discussion on the QCD axions as a dark matter, see refs.[39–41]).

Thus, the restriction in the generation of field excitation in FDM should only arise due to finite size effects and small strain amplitude (and of course due to short duration of GWs, which we discuss in Sect.IIB(ii)). Indeed, these are the two main competing factors which can affect the generation of field excitation at different radial distances r from the source. For small r , the finite size effects restrict the generation of field excitation for frequencies that are smaller than the cut-off frequency at 2-sphere for a given r , whereas for larger r , the strain amplitude of GWs becomes so small that it cannot generate field excitation. Therefore, the generation of field excitation in FDM is expected to occur only in a certain range of r , that is, in a *spherical shell* about the GW source.

The generated field excitations in the shell has higher energy density than the outer region of the shell. Therefore, as soon as these excitations arise in spherical shell, in order to minimize energy density of the field configuration, the field excitations start propagating out of the shell. These excitations are the perturbations in FDM (a superfluid medium) in terms of fluid velocity, energy density, and pressure on the top of a uniform medium with almost zero fluid velocity. They may have acoustic (linear) perturbations as well, which propagate in the fluid with the speed of sound. Additionally, as soon as GWs pass completely, the excited field in the shell starts rolling back toward the minimum of the effective potential, and oscillates about it. These various aspects make this phenomenon even more interesting.

In this work, we consider ultralight axion-like field as a field description for FDM. Our focus is to study the evolution of this field near a strong GW source. In the first part of the study, we show that a sustained spacetime oscillations can generate excitations in the field that initially has a uniform field configuration with small random fluctuations. These excitations are generated under the phenomenon of parametric resonance. Due to the spacetime oscillations, the field configuration mainly goes through two processes: first, the process of growth of some specific field-modes following the resonance conditions for the given spacetime oscillation frequency, and then the process of generation of various other field-modes due to non-linear evolution of the field. This, in general, may generate local superflow in FDM at a length scale smaller than f_{GW}^{-1} but bigger than the length scale of initial fluctuations. In the second part, we consider

a model GW waveform constructed using parameters of the observed waveform for a BBH merger, and show that the GWs produced by such source can also excite the field in a *spherical shell* about the source. These excitations arise toward the end of the merger and in some cases even in the ringdown phase of the merger, which may provide a distinct observable imprints on the measured GWs on Earth. By using a sine-Gaussian GW waveform, we also determine the parameter range of the waveform for which the resonance growth is possible in FDM. For the study, we solve the Klein-Gordon equation of motion for the field as in our case the length scale of evolution of the system is much smaller than the Compton wavelength m^{-1} of associated particles; the non-relativistic approximation, which gives the Schrödinger-Poisson equation of motion for FDM, is valid only for length scale larger than m^{-1} [1].

Recently, it has been shown that the presence of clouds of ultralight axion-like field around BHs lead to a suppression in the strain amplitude and frequency of GWs in the ringdown phase of the BBH merger [25]. This suppression increases with the physical characteristic parameters of the cloud such as mass parameter $\tilde{\mu}=GMm/\hbar c$ and amplitude of the field (where M is the total Arnowitt-Deser-Misner mass of gravitational system). For a range of values of such parameters of the cloud, the Bayesian analysis gives the suppression in the frequency of GWs between 2.1–8.6% [25]. Our results in the present work provide a possible explanation for such suppression due to the clouds. As mentioned earlier, in our case, the GWs passing through FDM lead to the generation of field excitations around the source that occurs toward the end and in the ringdown phase of the merger. Therefore, this should increase the total energy of the field configuration. As the energy of field configuration is increased due to GWs, therefore because of energy conservation, the GWs should lose their energy in these two phases of the merger, which leads to the suppression in strain amplitude and frequency of GWs as observed in ref.[25]. In this way, our study along with the study in ref.[25] open a new possibility of indirect detection of FDM and constraining such dark matter model by studying the discrepancy in between expected GW waveform from a well known GW source and the measured waveform on Earth. In the specific case of binary merger systems, this discrepancy must arise toward the end and in the ringdown phase of the merger. Thus, it provides a qualitatively distinct predictions for changes in the GW waveform compared to other prospects discussed earlier.

This paper is organized in the following manner. In Sec.II, we provide the field equation for FDM minimally coupled to gravity with oscillating spacetime metric. Then we consider two cases. In Sec.IIA, we consider a continuous GW waveform and show that this leads to the generation of field excitation induced by parametric resonance. Then in Sec.IIB, we again consider two

cases. In Sec.IIB(i), we consider a model GW waveform constructed using parameters of BBH merger, and show that this can lead to the generation of excitations in FDM in a *spherical shell* about the GW source, which are generated toward the end of the merger and in some cases even in the ringdown phase of the merger. In Sec.IIB(ii), by using sine-Gaussian GW waveform, we determine the *resonance growth zone* for FDM, for a parameter range of the waveform. Finally, we conclude in Sec.III.

II. FIELD EXCITATION IN FDM

To study the effects of spacetime oscillations on ultralight axion-like field ‘ a ’, we consider time-dependent perturbations in the Minkowski metric, such as $g_{\mu\nu}=\text{diag}(-1,1-h,1+h,1)$, where $h\equiv h(t,z)$ and $|h|<1$. The action of the field on the spacetime manifold with the given metric is [4]

$$S = \int d^4x \sqrt{-g} \left[-\frac{1}{2} F^2 g^{\mu\nu} \partial_\mu a \partial_\nu a - \mu^4 (1 - \cos a) \right], \quad (1)$$

where $g=\det(g_{\mu\nu})=-(1-h^2)$, and the parameter F has values in the range $10^{16}\text{GeV} \lesssim F \lesssim 10^{18}\text{GeV}$ [4]. Mass of the field ‘ a ’ is given by $m=\mu^2/F$ [4], where $m\sim 10^{-22}\text{eV}$ is taken in this study. The equation of motion for the field is given by [36, 42]

$$\square a - \frac{1}{F^2} \frac{dV}{da} = 0, \quad (2)$$

where the effective potential $V(a)=\mu^4(1-\cos a)$ and the covariant d’Alembertian is given by

$$\square a = \frac{1}{\sqrt{-g}} \partial_\mu \left(\sqrt{-g} g^{\mu\nu} \partial_\nu a \right). \quad (3)$$

In the expanded form, the field equation becomes

$$\frac{h_t a_t - h_z a_z}{h^{-1}(1-h^2)} - a_{tt} + \frac{a_{xx}}{1-h} + \frac{a_{yy}}{1+h} + a_{zz} - m^2 \sin a = 0, \quad (4)$$

where derivatives are defined as $\xi_\alpha = \partial \xi / \partial \alpha$, $\xi_{\alpha\alpha} = \partial^2 \xi / \partial \alpha^2$ for $\xi \equiv (h, a)$ and $\alpha \equiv (t, x, y, z)$.

A. With continuous GW waveform

We consider a continuous GW waveform with $h(t,z) = \varepsilon \sin(\omega(t-z))$, where ε and ω are the time-independent strain amplitude and angular frequency of GWs, respectively. We define $f(t,z) = 1-h(t,z)$. With this waveform, the above field equation becomes

$$\frac{\varepsilon^2 \omega \sin(2\omega(t-z))}{2f(t,z)f(-t,-z)} (a_t + a_z) - a_{tt} + \frac{a_{xx}}{f(t,z)} + \frac{a_{yy}}{f(-t,-z)} + a_{zz} - m^2 \sin a = 0. \quad (5)$$

This field equation leads to the phenomenon of parametric resonance [36], in which some specific momentum-modes of the field, following the respective resonance conditions, grow with time and lead to the field excitation.

The above equation can be used for the evolution of field ‘ a ’ around a continuous GW source. However, as the coefficient of second-order spatial derivative of field with respect to z is trivially one, i.e. non-oscillating, therefore the field-modes corresponding to z -axis do not grow resonantly. Thus, for simplicity of solving the above equation numerically, we take the following assumptions: (i) instead of considering three-dimensional space, we solve this equation on a two-dimensional surface by assuming that there is no variation of field along third axis (i.e., along z -axis), (ii) instead of solving it on a surface of 2-sphere, we solve it on a torus geometry, where we take lattice structure as a flat sheet that forms xy -plane ($z=0$ plane) and use periodic boundary conditions. Certainly, the quantitative values of our results could be affected due to this choice of boundary conditions, as discussed in some detail in ref.[36]. In the regime where finite size effects dominate, the *periodic* boundary conditions impose more restrictions in the generation of field excitations under the phenomenon of parametric resonance in comparison with the use of *fixed* boundary conditions [36]. However, other than this, these boundary conditions do not have any qualitative effect on the phenomenon. With these assumptions, the above equation reduces to

$$\frac{\varepsilon^2 \omega \sin(2\omega t)}{2f(t)f(-t)} a_{tt} - a_{tt} + \frac{a_{xx}}{f(t)} + \frac{a_{yy}}{f(-t)} - m^2 \sin a = 0, \quad (6)$$

where the function $f(t)=1-\varepsilon \sin(\omega t)$. We define dimensionless variables as $t'=mt$, $x'=mx$, $y'=my$, $z'=mz$, and $\omega'=\omega/m$. With these variables, the function $f(t)$ remains unchanged, i.e., $f(t')=f(t)$, and the equation of motion becomes

$$\frac{\varepsilon^2 \omega' \sin(2\omega' t')}{2f(t')f(-t')} a_{t't'} - a_{t't'} + \frac{a_{x'x'}}{f(t')} + \frac{a_{y'y'}}{f(-t')} - \sin a = 0. \quad (7)$$

We take the mass of the field as $m=10^{-22}\text{eV}$ [4], and a fix value of GW frequency as $f_{\text{GW}}=\omega/2\pi=250\text{ Hz}$ [43] which gives $\omega'=1.05\times 10^{10}$. For numerical simulation, the validity of the above equation demands that the time step of field evolution $\Delta t'$ should be $\Delta t' \ll 1/\omega'$. Therefore, we take $\Delta t'=3\times 10^{-12}$ as the minimum time step, and lattice spacing as $\Delta x'=\Delta y'=2\Delta t'$. With this, $\Delta t=2\times 10^{-5}$ s and $\Delta x=\Delta y=12$ km. For simulations, we consider $N=200$ lattice points in each spatial direction. Therefore, the total surface area of the torus will be $N^2 \Delta x \times \Delta y=5.76\times 10^6$ km². Note that to avoid finite size effects on the field evolution, the condition $L=N\Delta x \geq 2/f_{\text{GW}}$ should be satisfied [36], where L is the system size in each direction. For the given f_{GW} and N , the above condition becomes $\Delta x \geq 12$

km, where the chosen lattice spacing is already at the lowest threshold.

For an estimate of the strain amplitude ε , we adopt the following procedure. If we consider a 2-sphere around a GW source having the surface area given above, then the radius of that sphere will be $r=677$ km; we denote this radius by r_0 . (At such a distance from the source, spacetime curvature may affect the field evolution and also, there may be small deviation from the Newtonian approximation taken below. However, as the main focus of this work is to show the effects of spacetime oscillations on the field, such as resonance growth etc., which should not be affected due to the overall spacetime curvature, therefore for simplicity, we ignore this in our study.) Therefore, at this distance from the GW source, the strain amplitude will be given by $\varepsilon=h_e r_e/r_0$, where h_e is the strain amplitude measured on Earth and r_e is the distance between GW source and the Earth. We consider a particular GW source that has $h_e=1.0\times 10^{-21}$ and $r_e=410_{-180}^{+160}$ Mpc [43]. (These values are taken just for an estimate of ε , though the source in ref.[43] produces a time varying GWs, which is considered in the next subsection.) This gives $\varepsilon=0.019_{-0.009}^{+0.007}$.

With the given parameters of spacetime oscillations, we perform numerical simulations to solve Eq.(7). For simulations, we prepare an initial field configuration having field values close to the minimum of effective potential with small random fluctuations. These field fluctuations are necessary to excite the field as the spacetime oscillations only couple to the field through spacetime derivatives; see Eq.(7). These fluctuations are not unphysical, rather, can arise naturally due to thermal and/or quantum fluctuations. Since the minimum of effective potential is at $a=0$, therefore fluctuations in the field $a(x, y)$ at initial time are considered about $a=0$. For this, we consider the initial field configuration $a(x, y)$ which varies randomly on lattice points within the range $[-\beta, \beta]$.

We now estimate the possible range of β for FDM. The BBH merger event, which we have considered, has occurred at 410_{-180}^{+160} Mpc distance away from the Earth. Thus, at the time of event, the age of the Universe should be $12.46_{-0.52}^{+0.59}$ Byr. At this stage, the temperature of Universe could be roughly the same as at present, which is $T=2.73$ K. Therefore, we consider the temperature of Universe at the time of event as the present Universe temperature and assume that the temperature of FDM is also the same as that of the Universe. (However, it should be noted that the location where we are studying the phenomenon of field excitations being close to a strong gravitational field. Therefore, it is possible that temperature may be locally higher than the ambient temperature of the Universe, which may slightly raise the bound of β which we calculate here.)

The thermal energy at a temperature is given by T (we work in the unit system in which $k_B=c=\hbar=1$). Thus, in natural units, T is the amount of energy

available in the system to rotate the axion-like field ‘ a ’ uniformly to an angle β in a given volume $(\Delta x)^3$. Thus, by ignoring the gradient energy at the boundary of such rotated configuration arising due to fluctuation, we have the relation $(\Delta x)^3 \Delta V(a) = T$, where $\Delta V(a) = V(\beta) - V(0) = \mu^4(1 - \cos \beta)$. By using the series expansion of cosine function for small β in this relation, we obtain

$$\beta \approx \frac{1}{\mu^2} \left(\frac{2T}{(\Delta x)^3} \right)^{\frac{1}{2}}. \quad (8)$$

Putting $\mu^2 = 10^{-8} \text{ MeV}^2$ for $m = 10^{-22} \text{ eV}$ and $F = 10^{17} \text{ GeV}$, and the values of Δx and T as given above, give $\beta \approx 1.5 \times 10^{-22} \text{ rad}$. Whereas, for the given range of values of m and F , the values of β varies between 10^{-10} rad to 10^{-35} rad .

In simulations, β smaller than 10^{-7} rad (in orders of magnitude) goes beyond the smallest precision of computation for potential energy density. Therefore, we only can take $\beta = 10^{-7} \text{ rad}$ as the smallest value for the study. However, it should be noted that the phenomenon in which we are interested is independent from the choice of the initial fluctuations of field (of course, the quantitative values of the outcome depend on it). Therefore, in this subsection, where we study a general possibility of parametric resonance in FDM, we take $\beta = \pi/10$, a greatly large value as a choice, and comment on the results for lower values of β . Whereas, in the next subsection, where we deal with BBH merger case, we take $\beta = 10^{-7} \text{ rad}$ – the smallest value which can be taken for the study – and present the results. In most of the cases, we present results in terms of percentage growth in potential energy density due to passing of GWs, which we show to be roughly independent from the choice of β . Therefore, we hope that the presented results will be valid even for the actual value of β as estimated above.

We utilize the periodic property of the effective potential, i.e., its invariance under $a \rightarrow a + 2\pi$, while calculating certain quantities such as the total energy density. Following this property of effective potential, we bring back the field within the range $[-\pi, \pi]$ if it goes beyond this range during the evolution. This ensures that the gradient energy is calculated correctly. We numerically solve Eq.(7) on torus with the given initial field configuration by using the second-order Leapfrog method [44].

In earlier work [36], it has been shown that a sustained spacetime oscillations can excite an initial field configuration, in which some specific momentum-modes of the field grow following the resonance conditions for the given oscillation frequency ω . These field excitations are induced by the phenomenon of parametric resonance. Under this phenomenon, at the early stage of the generation of field excitation, the whole field configuration acquires some specific momentum-modes with growing amplitude with time. However, at later times, the field

dynamics becomes much more complicated because of non-linearity of the field evolution, due to which various other momentum-modes of the field are also generated (modes that are not even related with the resonance conditions). To show this for the present case, we write the field $a \equiv a(x, y)$ in terms of components $a_1 \equiv a_1(x, y)$ and $a_2 \equiv a_2(x, y)$, where $a_1 = \cos a$ and $a_2 = \sin a$; here we are representing the angular field a in terms of vector $a_1 \hat{i} + a_2 \hat{j}$ in the internal space of the field. Furthermore, to understand the field configuration at each time, we perform Fourier transform of the components a_1 and a_2 as

$$\tilde{a}_i(\vec{k}, t) = \frac{1}{\mathcal{A}} \int_{b.c.} d^2\vec{x} a_i(\vec{x}, t) e^{i\vec{k} \cdot \vec{x}}; \quad i = 1, 2, \quad (9)$$

where \mathcal{A} is the total area of the system, *b.c.* stands for *boundary condition*, and $\vec{k} = k_x \hat{x} + k_y \hat{y}$, $\vec{x} = x \hat{x} + y \hat{y}$ are the momentum and position vectors, respectively.

In Fig.1, we plot modulus of $\tilde{a}_i(\vec{k}, t)$ for two time steps of the field evolution, at $t=0$ (upper panel) and at $t=1.4 \text{ s}$ (lower panel), in $(k_x/\omega, k_y/\omega)$ -plane. In the left panel, we plot $|\tilde{a}_1(\vec{k}, t)|$, and in the right panel, $|\tilde{a}_2(\vec{k}, t)|$. For the simulation, the parameters of spacetime oscillations are taken as $f_{GW} = 250 \text{ Hz}$ and $\varepsilon = 0.026$ (maximum possible value of ε estimated earlier). As mentioned earlier, we consider the initial field configuration $a(x, y)$ which varies randomly around zero, so naturally the distribution of $|\tilde{a}_1(\vec{k}, t)|$ takes a peak at zero-momentum with a value of about 1, while the distribution of $|\tilde{a}_2(\vec{k}, t)|$ shows some random variations depending on the initial random fluctuations of the field, with a very small magnitude. This represents the zero-momentum BEC state of FDM, which depends on the sequence of random numbers used to generate the initial field configuration. At time $t=1.4 \text{ s}$, due to sustained spacetime oscillations, some specific momentum-modes of a_2 have grown around $k_x \approx \omega/2$, $k_y \approx 0$ ($k_x \approx 0.5 \text{ peV}$ for the given ω) with peak value ~ 0.6 , while the magnitude of zero-momentum mode of a_1 has decreased. This may generate a superflow in FDM in some local regions that have length scale smaller than f_{GW}^{-1} (half-wavelength of the generated field-modes) but bigger than Δx (the length scale of initial fluctuations) such that the net global flow is zero. We have seen a noticeable growth in these momentum-modes starting from the time $t \simeq 0.9 \text{ s}$ which continues to grow till the time $t = 1.4 \text{ s}$. At later times, with further evolution, the field acquires various other momentum-modes because of non-linear field dynamics.

As mentioned earlier, this growth in the specific momentum-modes is occurring due to parametric resonance of the field, where these modes are generated following the respective resonance conditions, that is, the relation between k_x , k_y , m , and ω . We determine the resonance conditions for Eq.(7) by writing in the momentum-space and then linearizing it; see ref.[36] for more details. We find that the resonance conditions for

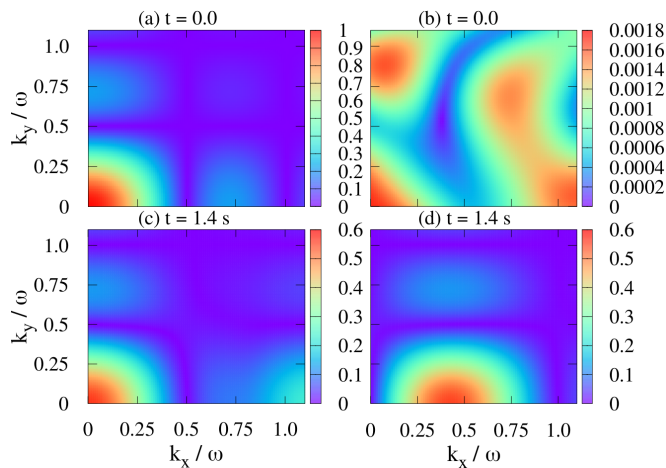


FIG. 1: Figure shows the distribution of $|\tilde{a}_1(\vec{k}, t)|$ (left panel) and $|\tilde{a}_2(\vec{k}, t)|$ (right panel) at initial time and at time $t=1.4$ s. The parameters of spacetime oscillations are $f_{GW}=250$ Hz and $\varepsilon=0.026$. Figure clearly shows that under the spacetime oscillations the initial field configuration (a_1, a_2) that has dominantly zero-momentum mode is excited to acquire higher momentum-modes following the resonance condition $k_x \approx \omega/2$, $k_y \approx 0$.

Eq.(7) follow the relation $k_x^2 + k_y^2 + m^2 \approx (n\omega/2)^2$, where $n=1, 2, 3, \dots$. Since in our case $\omega \gg m$, therefore the above relation reduces to $k_x^2 + k_y^2 \approx (n\omega/2)^2$: an equation of circle in the momentum-space. The growth in momentum-modes in Fig.1 clearly validates this relation.

Due to the generation of field excitation, the energy density of the system keeps on increasing with time and reaches a maximum value. In simulation, we calculate the total energy density of the system $T_{00}^{(a)} = \mu^4 T_{00}'^{(a)}$ at each time, where

$$T_{00}'^{(a)} = \frac{a_{t'}^2}{2} + \frac{a_{x'}^2}{2f(t')} + \frac{a_{y'}^2}{2f(-t')} + (1 - \cos a). \quad (10)$$

To calculate these terms, we utilize the periodic property of the effective potential as mentioned earlier, under which we bring back the field within the range $[-\pi, \pi]$ if it goes beyond this during the evolution. We calculate average values of all above terms on two-dimensional lattice at each time. We see the growth in each term of the energy density due to the generation of field excitations induced by spacetime oscillations. In Fig.2, we show the time evolution of average potential energy density (multiplied by μ^{-4}) for the given value of f_{GW} and ε (since the scale of the potential energy density is set by μ , we choose to measure the potential energy density in the units of μ^4). Since in the initial field configuration, the field varies randomly between the range $[-\beta, \beta]$ where β is a small number, the average value of the potential energy density is initially very small. Under the sustained spacetime oscillations, when the field achieves full excitations, it covers the whole field-space in the range $[-\pi, \pi]$.

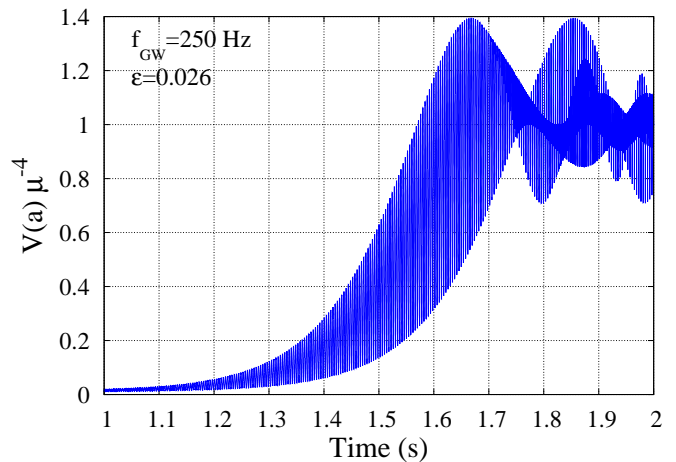


FIG. 2: Figure shows the growth in average potential energy density (multiplied by μ^{-4}) under the sustained spacetime oscillations.

In such a situation, the average value of $V(a)\mu^{-4}$ becomes ~ 1 as can be seen in the figure.

We find that, the total energy density of the field achieves roughly two orders of magnitude growth from the initial value. As mentioned earlier, for this simulation, we have taken $\beta=\pi/10$, which gives a large initial fluctuations to the field. Instead of it, if we take $\beta=\pi/200$, it gives smoother initial fluctuations to the field due to which the total energy density of the initial field configuration is reduced compared to the former case. We see that even in the latter case, the resonance growth of the field begins around the same time as in the former case, that is, at time $t \approx 0.9$ s. However, due to the lower initial energy density in the latter case, the field takes longer time to achieve full excitations; in the former case, it takes the time $t \approx 1.7$ s, while in the latter case, it takes $t \approx 2.6$ s, to achieve full excitations.

We also see that increasing values of f_{GW} and ε reduces the time to achieve field excitations (if the appropriate momentum-modes of the field corresponding to frequency ω are present initially). Thus, a stronger GW source can excite the field in relatively shorter time. As discussed earlier, as soon as the spacetime oscillations stop, the field starts rolling-back toward the minimum of the effective potential, which leads to the oscillations in the field about the minimum.

B. With time varying GW waveform

(i) BBH merger GW waveform

In the previous case, we have taken a continuous GW waveform that enables the field ‘a’ to excite under the phenomenon of parametric resonance. However, BBH and BNS mergers do not produce a continuous GWs.

Rather, these sources produce a time varying GWs whose amplitude and frequency increase until the merger is completed. Therefore, the phenomenon of generation of field excitation may become much more complicated in this case. In this subsection, a time varying GW waveform is considered to study the field excitations near a strong GW source. For simplicity, the GW waveform is taken to be

$$\begin{aligned} h_e &= 10^{-21} [h_a e^{h_b t} \sin(\omega t)], & t \leq t_0, \\ h_e &= 10^{-21} [h_c e^{-h_d(t-t_0)} \sin(\omega t)], & t > t_0, \end{aligned} \quad (11)$$

where $\omega = 2\pi f_{GW}$, $f_{GW} = \exp(f_a e^{f_b t} + f_c)$, and $(h_a, h_b, h_c, h_d, f_a, f_b, f_c, t_0)$ are the phenomenological parameters to be fitted using a known GW waveform. (Note that in general, the strain amplitude of GWs produced by BBH or BNS mergers are not spherically symmetry about the source [45]. However, for simplicity here we ignore this, and proceed by considering a spherically symmetric GW strain amplitude about the source. We also ignore the cross-polarization component of GWs.) We determine parameters of the above function such that h_e shows a qualitatively similar variation as the strain amplitude for a known GW source. For this, we consider the GW source GW150914 [43], and model the waveform with the above function. By taking some limiting values of h_e from the actual waveform, we obtain $f_a = 2.9 \times 10^{-8}$, $f_b = 42.5 \text{ s}^{-1}$, $f_c = 3.465$, and the remaining parameters, for the two possible values of the merger time t_0 , as given in the table-I. The values of h_d are taken such that h_e becomes close to

	h_a	$h_b(\text{s}^{-1})$	h_c	$h_d(\text{s}^{-1})$	$t_0(\text{s})$
Set-I	7.7×10^{-4}	17.5	1.3	300.0	0.425
Set-II	1.1×10^{-3}	16.4	1.3	500.0	0.43

TABLE I: Table provides values of some parameters of GW waveform, given in Eq.(11), for two possible values of the merger time t_0 .

zero at time $t=0.44 \text{ s}$ [43] for both the cases. With this, the ringdown phase of the merger lasts longer for Set-I parameters than for Set-II parameters.

The GW waveform given by the above function is not exactly the same as that produced by GW150914, though the qualitative variation in the strain amplitude and frequency of the waveform is similar to this source [43]. It should be noted that the focus of the present study is to demonstrate a general possibility of generation of field excitation due to passing of GWs, without focusing on any particular GW source. Certainly, a detailed structure of the GW waveform can affect the generation of field excitations quantitatively. In fact, we show that our results are highly sensitive to the parameters of the GW waveform used for the simulation.

To perform simulations, in this case also, we continue with the assumptions that there is no variation of the

field along z -direction (along r in spherical polar coordinates) and the consideration of the lattice structure as a flat sheet forming $z=0$ plane with periodic boundary conditions. Under these assumptions and in terms of dimensionless variables, Eq.(4) becomes

$$\frac{h_{t'} a_{t'}}{h^{-1}(1-h^2)} - a_{t't'} + \frac{a_{x'x'}}{1-h} + \frac{a_{y'y'}}{1+h} - \sin a = 0, \quad (12)$$

where $h = h_e r_e / r$, and from Eq.(11),

$$\begin{aligned} h_{t'} &= \mathcal{R} h_a e^{h_b t'} [h'_b \sin(\omega' t') + \Omega], & t' \leq t'_0, \\ h_{t'} &= \mathcal{R} h_c e^{-h'_d(t'-t'_0)} [-h'_d \sin(\omega' t') + \Omega], & t' > t'_0, \end{aligned} \quad (13)$$

where $\mathcal{R} = 10^{-21} r_e / r$, $h'_b = h_b / m$, $h'_d = h_d / m$, $t'_0 = m t_0$, $\Omega = (\omega' + \omega'_t t') \cos(\omega' t')$, $\omega'_t = \omega' f_a f'_b e^{f'_b t'}$, and $f'_b = f_b / m$. Using these parameters of GWs, we perform simulations to solve Eq.(12). We take the same lattice spacing Δx (that gives $r = r_0$) and time step Δt as used before, and $\beta = 10^{-7}$ rad for the initial field fluctuations. We take the maximum possible value of r_e for the source GW150914, which is $r_e = 570 \text{ Mpc}$ [43]. We follow the same procedure of calculating r and strain amplitude h as used in the last subsection.

In Fig.3, we plot the time evolution of average potential energy density (multiplied by μ^{-4}) for the given sets of parameters. Curve $1h$ corresponds to the case when the actual h has been taken (as defined in Eq.(11)), while curve $2h$ corresponds to the case when factor two is multiplied into h . In the upper panel, the plot shows the time evolution of the potential energy density for Set-I GW waveform, which is only plotted for the case of $2h$ (brown). For $1h$, the overall growth in potential energy density is approximately 1.1% from the initial value, which is very small to show in the plot. The growth in the potential energy density for the case of $2h$ is approximately 3.9%. In the lower panel, the plot shows the time evolution of the potential energy density for Set-II GW waveform for $1h$ (blue) and $2h$ (red) cases. In these two cases, there are approximately 5.6% and 24.3% overall growth in the potential energy density from the initial value at the given constant r -hypersurface. The curve $2h$ in the plot indicates that a relatively strong GW source can cause a very large growth in the energy density of FDM. The percentage growth in total energy density is also in the same order as that for potential energy density.

The growth in the potential energy density for Set-I and Set-II has basically two distinct features: (i) the overall growth in the potential energy density, and (ii) the time-domain of the occurrence of these growths. The overall growth for Set-I is lesser than the growth for Set-II. This is because for Set-II, a large strain amplitude and frequency are simultaneously present in the waveform toward the end of the merger to generate large excitations in FDM, which is somewhat absent for Set-I. On the other

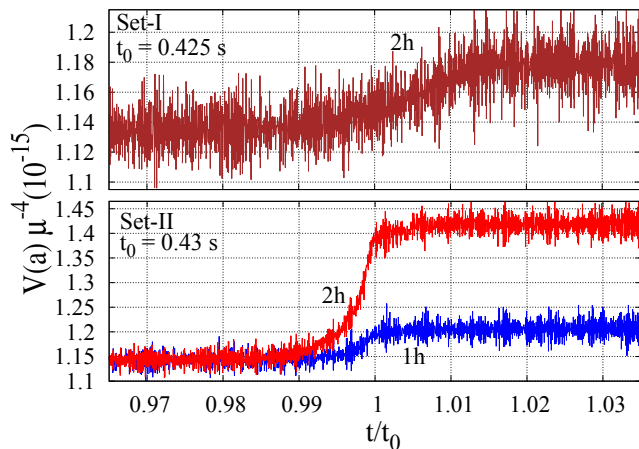


FIG. 3: Figure shows the growth in average potential energy density (multiplied by μ^{-4}) at $r=r_0$ hypersurface for Set-I (upper panel) and Set-II (lower panel). These growths arise around t_0 time, that is, toward the end and in the ringdown phase of the merger. Curve $1h$ corresponds to the case when the actual h has been taken, while curve $2h$ corresponds to the case when factor two is multiplied into h .

hand, for Set-I, since the ringdown phase persists for a longer time, the growth in potential energy density continues even after time t_0 [$0.98t_0 \lesssim t \lesssim 1.013t_0$], which is quite different from the case of Set-II in which growth is very rapid around time t_0 [$0.98t_0 \lesssim t \lesssim t_0$] and stops quickly after it. All this suggests that the generation of field excitations is highly sensitive to the parameters of the GW waveform, which based on these parameters can be generated toward the end as well as in the ringdown phase of the merger.

We also study the distribution of field-modes in (k_x, k_y) -plane at t_0 time, as done in Fig.1. We find that for each case in Fig.3, the initial distribution of $|\tilde{a}_2(\vec{k}, t)|$ is redistributed at time t_0 without much growth, and takes peak at a higher momentum causing growth in energy density of FDM.

We have verified that the percentage growths discussed in Fig.3 are independent from the strength of the initial field fluctuations, that is, from the choice of β . We find that for the range of β from 10^{-1} to 10^{-7} rad, the percentage growth in potential energy density for Set-II parameters (with $1h$) *randomly* varies between 5.1–5.7% (an extremely small *random* variation for many orders of magnitude change in β), which shows that it is almost independent from the choice of β . It indicates that our results could be valid even for the actual value of β , i.e. for $\beta \sim 10^{-22}$ rad, as estimated previously for FDM.

It should be noted that due to finite size effects, the field cannot achieve excitations until the frequency of GWs becomes equal or exceeds the lowest frequency cut-off $f_{GW}=250$ Hz for this hypersurface. Certainly, for higher r -hypersurfaces, the frequency cut-off will be lesser than $f_{GW}=250$ Hz, which would provide a larger

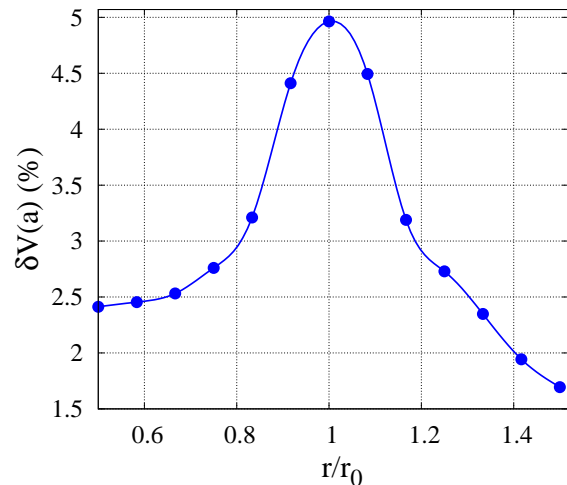


FIG. 4: Figure shows the percentage growth in average potential energy density $\delta V(a)$ at different r from GW source; $r_0=677$ km. This entire curve is a result of a combination of finite size effects and strain amplitude, which shows that only in a *spherical shell* about the GW source, field excitations can be generated.

time-domain for the field to achieve excitations. However with increasing r , the strain amplitude also decreases, which can suppress the generation of field excitation. On the other hand, although the strain amplitude becomes larger for smaller r , the finite size effects suppress the generation of excitations. Therefore, the field excitations are expected to be generated in a *spherical shell* about the GW source with maximum excitation at an optimum radial distance r . Although this investigation requires full (3+1)-dimensional simulations, in the given simulation setup, we now show that our this expectation is true.

In Fig.4, we plot the percentage growth in average potential energy density $\delta V(a) = \frac{V(t>t_0) - V(t=0)}{V(t=0)} \times 100\%$ at different r . The simulations are performed using parameters of Set-II. However, for this study, we stop the space-time oscillations after time t_0 for each r to avoid any ambiguity in the choice of h_d that may arise while simulating hypersurfaces for $r < r_0$. This consideration does not affect the physical aspects in which we are interested. To change r in the simulations, we change Δx ($=\Delta y$). As the maximum momentum-mode present in the initial field configuration is given by $k_{max}=2\pi/\Delta x$, therefore with the change in Δx , the momentum-modes present in the initial field configuration also change. This may affect the resonance process quantitatively. However, its effects should not be very significant as the overall change in k_{max} is only between 69.8 to 209.3 peV for the given range of Δx (6.0 – 18.0 km) in Fig.4. As discussed above, the entire curve in Fig.4 is a result of a combination of finite size effects and strain amplitude, which clearly shows that the field excitations can arise only in a *spherical shell* about the GW source.

Throughout the evolution, the field remains in the linear regime, and hence the momentum-modes of the field corresponding to z -axis will not be affected by the growth of k_x and k_y modes of the field. Therefore, in this case, our (2+1)-dimensional simulation is a reasonable approximation to the full (3+1)-dimensional simulations. However, as mentioned earlier, the generation of field excitation in FDM should cause a loss in GW energy due to energy conservation. Therefore, this process of generation of field excitation should modify the actual waveform produced by the GW source, especially toward the end of the merger. Therefore, to study the back-reaction of the generated field excitations, in determining the actual changes in the GW waveform, one needs to solve full Einstein's equation, which is not our focus in this work.

In this study, the results are presented using a model GW waveform that is suitable for an observed GW waveform on Earth. We have considered it as an actual waveform produced by a source, and performed the simulations. With the simulation results, we then conclude that the GWs can generate field excitations in FDM around the source, which would modify the GW waveform due to energy loss. Thus, this study suggests that the GWs observed on Earth may have already been affected due to the presence of FDM. A detailed study will reveal whether such a change in the GW waveform can be observed experimentally, and if it does, it will indirectly show the existence of FDM in the intermediate region between the GW source and the Earth.

(ii) Sine-Gaussian GW waveform

In the previous subsection, we have shown, by using a specific GW source, that a time varying GWs can generate field excitations in FDM. Indeed, some GW sources, such as core-collapse supernovae (CCSNe), generate transient GWs whose duration may vary from one source to another. We now show that the duration of GWs may affect the generation of field excitations in FDM. To analyze it, we consider a sine-Gaussian function as an *ad hoc* GW waveform [46–50], which is also used to model the GW waveform produced by CCSNe [49, 50]. This waveform is given by

$$h = h_0 \exp(-(t - t_0)^2/\tau^2) \sin(2\pi f_{GW} t), \quad (14)$$

where h_0 is an amplitude scale factor, t_0 is the arrival time of GW signal, τ quantifies the duration of signal, and f_{GW} is the frequency of GWs. For simplicity, we again ignore the cross-polarization component of GWs.

In this case also, we use the same simulation parameters as used in the last subsections to solve Eq.(12). For the study, we take $t_0=0.3$ s, and $f_{GW}=\{250, 500\}$ Hz. The value of t_0 is chosen sufficiently large compared to τ so that its value cannot affect the growth in the average potential energy density. Our focus is to determine the

parameter range of this waveform for which FDM can be excited. A GW waveform with arbitrarily small τ cannot generate resonance growth in FDM. The same is also true for a waveform with arbitrarily small h_0 . Therefore, in the parameter space (h_0, τ) , for each frequency f_{GW} , there should be *resonance growth zone* and *growth forbidden zone* partitioned by a curve whose horizontal and vertical asymptotes are at $h_0 \neq 0$ and $\tau \neq 0$, respectively. As already discussed, the frequency cutoff to generate resonance growth is set by the finite size effects on the respective r -hypersurface from the source.

In Fig.5, we plot the *resonance cutoff* points in parameter space (h_0, τ) for each f_{GW} , which divide the parameter region of possible resonance growth to the *growth forbidden zone*. In the simulations, we observe resonance growth only for those h_0 that have value higher than the plotted points for each τ . Thus, the *resonance growth zone* covers the region *above* these points for the respective f_{GW} . With increasing values of h_0 and τ above these points, the overall growth in average potential energy density increases. The errors in the plot indicate the uncertainty in determination of value of h_0 for which there is no resonance growth. This plot clearly indicates that the generation of field excitations in FDM is only possible with the GWs that have a significant duration and strain amplitude. It is also clear from Fig.5 that the *resonance growth zone* is strongly reduced toward smaller τ by decreasing frequency, which is depicted by arrows in the plot. The plotted points for $f_{GW}=500$ Hz can be best fitted by the function $h_0=10^{-3} \left(5.3(\tau-3.3 \times 10^{-3})^{-0.84} + 2.0 \right)$ indicating to have the lowest cutoff for τ as well as h_0 to generate resonance growth at the two extremes, $\tau \rightarrow 0$ and $\tau \rightarrow \infty$, respectively.

The result presented in Fig.5 has important phenomenological implications for CCSNe. It may be possible that some CCSNe generate GWs whose parameters are such that they are capable of generating field excitations in FDM in a *spherical shell*. It is expected that the GWs produced by a CCSN carry the information of explosion mechanism, more specifically, the magnitude and character of deviation of the core from its spherical symmetry [49]; for a review, see [51]. Thus, with the detection of the GWs produced by CCSNe, one is expected to be able to probe the dynamics of deep inside the core of SNe. However, as we argue that GWs produced by CCSNe, in some parameter range, could excite FDM present in the outer space, hence should lose some energies due to energy conservation. Therefore, this process may hide some relevant information of CCSNe that are expected to be studied by detecting GWs. We will explore this in more detail in our future work.

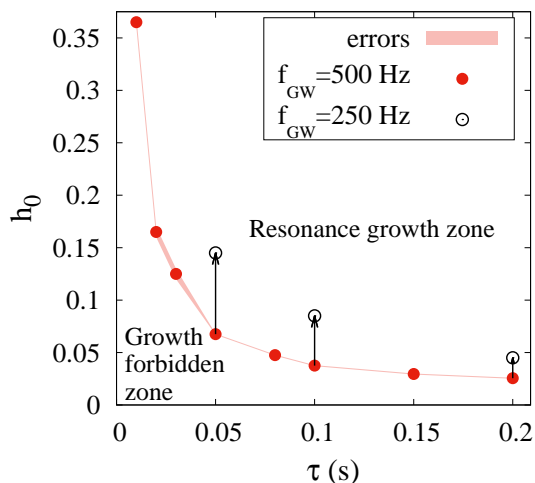


FIG. 5: Figure shows the *resonance growth zone* and *growth forbidden zone* for FDM in parameter space (h_0, τ) . The analysis is done for $f_{GW}=250$ Hz (empty circles) and $f_{GW}=500$ Hz (filled circles), at r_0 hypersurface; $r_0=677$ km. The *resonance growth zone* covers the region above the plotted points for the respective f_{GW} . This zone is strongly reduced toward smaller τ by decreasing frequency, which is depicted by arrows. The errors in the plot indicate the uncertainty in determination of value of h_0 for which there is no resonance growth.

III. CONCLUSIONS

In this work, we have shown that strong gravitational waves (GWs) can generate field excitations in fuzzy dark matter (FDM) in *spherical shell* about the GW source. The field description for FDM is considered as an ultralight axion-like field having mass $m \sim 10^{-22} \text{eV}$, where initially the field is taken at the minimum of effective potential with small random fluctuations. These generated excitations can lead to the generation of local superflow in FDM. As soon as these excitations arise, in order to minimize the energy density of the field configuration, they start propagating out of the shell as the perturbations in FDM. These excitations may have acoustic (linear) perturbations as well, which propagate with the speed of sound in medium.

We have shown, by using a model GW waveform suitable for a binary black hole (BBH) merger, that GWs can generate field excitations in FDM toward the end and in the ringdown phase of the merger. Due to energy conservation, while generating these excitations, GWs will lose their energy in these two phases of the merger, due to which GW waveform should get modified. Thus, our results can provide a qualitatively distinct prediction for the presence of FDM around the GW source than the other prospects discussed earlier in literature. This may be observed in the measurement of GWs on Earth, which requires a detailed investigation. A detailed study in ref.[25] shows a suppression in the strain amplitude and frequency of GWs in the ringdown phase of BBH merger

due to the presence of clouds of ultralight axion-like field. A possible explanation for such suppression can be given due to the phenomenon discussed in the present work.

The generation of field excitations is not only limited to the above choice of parameters of field and GW source, rather, can be possible for a wide range of masses of axion-like field and for any strong GW source. Indeed, we have also shown that a sine-Gaussian GW waveform can generate field excitations in FDM, and determined the *resonance growth zone* for a parameter range of this waveform. Thus, the main criteria, we obtain to generate the field excitations in FDM, are: (i) the angular frequency of GWs should be $\omega \geq m$, (ii) the surface area of the 2-sphere about the source must be large enough to avoid finite size effects, and (iii) the strain amplitude on that 2-sphere, and the duration of GWs, should be large enough to generate field excitations.

ACKNOWLEDGEMENTS

We are very grateful to Ajit M. Srivastava and Bharat Kumar for very useful discussions, suggestions, and comments on the manuscript. We also would like to thank A.P. Balachandran, T.R. Govindarajan, P.S. Saumia, Abhishek Atreya, Minati Biswal, and Subhrooneel Chakrabarti for useful discussions and comments on the work.

-
- [1] W. Hu, R. Barkana, and A. Gruzinov, Phys. Rev. Lett. **85**, 1158 (2000).
 - [2] B. Li, T. Rindler-Daller, and P.R. Shapiro, Phys. Rev. D **89**, 083536 (2014).
 - [3] T.R. Govindarajan and N. Kalyanapuram, Mod. Phys. Lett. A **34**, 1950330 (2019).
 - [4] L. Hui, J.P. Ostriker, S. Tremaine, and E. Witten, Phys. Rev. D **95**, 043541 (2017).
 - [5] H.-Y. Schive, T. Chiueh, and T. Broadhurst, Nature Phys **10**, 496 (2014).
 - [6] R. Brito, V. Cardoso, and P. Pani, *Superradiance: New Frontiers in Black Hole Physics*, 2nd ed., Lecture Notes in Physics Vol. **971** (Springer, Cham, 2020).
 - [7] S.R. Dolan, Phys. Rev. D **87**, 124026 (2013).
 - [8] R. Brito, V. Cardoso, and P. Pani, Class. Quantum Grav. **32**, 134001 (2015).
 - [9] G. Ficarra, P. Pani, and H. Witek, Phys. Rev. D **99**, 104019 (2019).
 - [10] D. Baumann, H.S. Chia, J. Stout, and L.t. Haar, JCAP **12**, 006 (2019).
 - [11] V. Cardoso, P. Pani and T.-T. Yu, Phys. Rev. D **95**, 124056 (2017).
 - [12] F.V. Day and J.I. McDonald, JCAP **10**, 051 (2019).
 - [13] A. Arvanitaki and S. Dubovsky, Phys. Rev. D **83**, 044026 (2011).
 - [14] A. Arvanitaki, M. Baryakhtar, and X. Huang, Phys. Rev. D **91**, 084011 (2015).

- [15] R. Brito, S. Ghosh, E. Barausse, E. Berti, V. Cardoso, I. Dvorkin, A. Klein, and P. Pani, *Phys. Rev. D* **96**, 064050 (2017).
- [16] O.A. Hannuksela, K.W.K. Wong, R. Brito, E. Berti, and T.G.F. Li, *Nat. Astron.* **3**, 447 (2019).
- [17] S. D'Antonio et al., *Phys. Rev. D* **98**, 103017 (2018).
- [18] M.J. Stott and D.J.E. Marsh, *Phys. Rev. D* **98**, 083006 (2018).
- [19] M. Isi, L. Sun, R. Brito, and A. Melatos, *Phys. Rev. D* **99**, 084042 (2019).
- [20] S. Ghosh, E. Berti, R. Brito, and M. Richartz, *Phys. Rev. D* **99**, 104030 (2019).
- [21] J. Zhang and H. Yang, *Phys. Rev. D* **99**, 064018 (2019).
- [22] K.K.Y. Ng, M. Isi, C.-J. Haster, and S. Vitale, *Phys. Rev. D* **102**, 083020 (2020).
- [23] K.K.Y. Ng, O.A. Hannuksela, S. Vitale, and T.G.F. Li, *Phys. Rev. D* **103**, 063010 (2021).
- [24] Q. Yang, L.-W. Ji, B. Hu, Z.-J. Cao, and R.-G. Cai, *Res. Astron. Astrophys.* **18**, 065 (2018).
- [25] S. Choudhary, N. Sanchis-Gual, A. Gupta, J.C. Degollado, S. Bose, and J.A. Font, *Phys. Rev. D* **103**, 044032 (2021).
- [26] D. Baumann, H.S. Chia, and R.A. Porto, *Phys. Rev. D* **99**, 044001 (2019).
- [27] E. Berti, R. Brito, C.F.B. Macedo, G. Raposo, and J.L. Rosa, *Phys. Rev. D* **99**, 104039 (2019).
- [28] D. Baumann, H.S. Chia, R.A. Porto, and J. Stout, *Phys. Rev. D* **101**, 083019 (2020).
- [29] M. Kavic, S.L. Liebling, M. Lippert, and J.H. Simonetti, *JCAP* **08**, 005 (2020).
- [30] T.K. Poddar, S. Mohanty, and S. Jana, *Phys. Rev. D* **101**, 083007 (2020).
- [31] B.C. Seymour and K. Yagi, *Phys. Rev. D* **102**, 104003 (2020).
- [32] B.J. Kavanagh, D.A. Nichols, G. Bertone, and D. Gaggero, *Phys. Rev. D* **102**, 083006 (2020).
- [33] J. Huang, M.C. Johnson, L. Sagunski, M. Sakellariadou, and J. Zhang, *Phys. Rev. D* **99**, 063013 (2019).
- [34] G. Bertone et al., *SciPost Phys. Core* **3**, 007 (2020).
- [35] J.-F. Fortin et al., *Int. J. Mod. Phys. D* **30**, 2130002 (2021).
- [36] S.S. Dave and S. Digal, *Phys. Rev. D* **103**, 116007 (2021).
- [37] A. Arvanitaki, S. Dimopoulos, S. Dubovsky, N. Kaloper, and J. March-Russell, *Phys. Rev. D* **81**, 123530 (2010).
- [38] E.G.M. Ferreira, *Astron. Astrophys. Rev.* **29**, 7 (2021).
- [39] J. Preskill, M.B. Wise, and F. Wilczek, *Phys. Lett. B* **120**, 127 (1983).
- [40] L.F. Abbott and P. Sikivie, *Phys. Lett. B* **120**, 133 (1983).
- [41] M. Dine and W. Fischler, *Phys. Lett. B* **120**, 137 (1983).
- [42] S. Carroll, *Spacetime and Geometry; An Introduction to General Relativity* (Addison Wesley, Reading, MA, 2004).
- [43] B.P. Abbott et al. (LIGO Scientific and Virgo Collaborations), *Phys. Rev. Lett.* **116**, 061102 (2016).
- [44] W.H. Press, S.A. Teukolsky, W.T. Vetterling, and B.P. Flannery, *Numerical Recipes in Fortran 77; The Art of Scientific Computing*, 2nd ed. Vol. 1 (Syndicate, New York and Melbourne, 1997).
- [45] L. Blanchet, *C. R. Physique* **20**, 507 (2019).
- [46] B.P. Abbott et al., *Phys. Rev. D* **80**, 102001 (2009).
- [47] J. Abadie et al., *Phys. Rev. D* **81**, 102001 (2010).
- [48] J. Abadie et al., *Phys. Rev. D* **85**, 122007 (2012).
- [49] B.P. Abbott et al., *Phys. Rev. D* **94**, 102001 (2016).
- [50] B.P. Abbott et al., *Phys. Rev. D* **101**, 084002 (2020).
- [51] K. Kotake, *C. R. Physique* **14**, 318 (2013).